

Topological Optimization of Damping Layout for Minimized Sound Radiation of an Acoustic Black Hole Plate

Li Ma and Li Cheng*

Department of Mechanical Engineering, The Hong Kong Polytechnic University, Hong Kong

E-mail: li.cheng@polyu.edu.hk

Abstract: Damping material is one of the essential components to achieve effective Acoustic Black Hole (ABH) phenomena. Alongside the expected energy absorption by the viscoelastic coating, recent research revealed its adverse effect in increasing the sound radiation efficiency of ABH structures. The conflicting role that damping layers play calls for a balanced and meticulous design of their deployment to draw the best possible vibration or acoustic benefit. This paper proposes a general methodology for optimizing the layout of damping layers coated on the surface of an ABH plate through topological optimization. By combining a semi-analytical wavelet plate model with an optimizer, the sound radiation into a free space by the ABH plate is minimized at either a given frequency or within a frequency band. Results show that through optimization, a reduced sound power can be achieved, as compared with the intuitive coating at the central area of the ABH indentation. While the low frequency sound power reduction is due to the impaired structural vibration, the optimization-induced reduction in the radiation efficiency is shown to be the dominant factor that contributes to the minimization of the sound power at high frequencies. Changes in the topology of the coating, in relation to the optimization objective, are observed and interpreted. It is shown that the optimized coating area for acoustic optimization tends to be further away from the center of the indentation, in contrast to the case for structural vibration optimization. The optimized configuration warrants a systematic reduction of the sound

radiation efficiency, as evidenced by a weakened vibration level of the supersonic components of the plate.

Keywords: 2-D semi-analytical model; topological optimization; Acoustic Black Hole (ABH)

1. Introduction

Controlling sound radiation of vibrating structures is an important research topic for many engineering applications. Among existing approaches, viscoelastic coating is one of the popular options to achieve vibration and sound radiation reductions through increasing structural damping in the system. Conventional structures, however, usually require a sufficient amount of damping material in order to increase the system damping up to an appreciable level. On the contrary, recent research demonstrated that, through embracing acoustic black hole (ABH) principle in the structural design, it is possible to conceive lightweight structures with only a small amount of damping materials to achieve appreciable vibration [1-3] and acoustic [4, 5] benefits.

ABH phenomenon takes effect in a thin-walled structure whose thickness profile is shaped according to a power-law relationship. Reaching the thin tip of an ABH beam or the indentation center of an ABH plate, the phase velocity of flexural waves gradually decreases, eventually to zero theoretically, alongside a drastic compression of waves and an amplification of the vibration amplitude. However, the inevitable residual thickness of the ABH, referred to as thickness truncation, generates wave reflections which adversely undermine the energy focalization effect. As a counter measure, the deposition of a thin layer of viscoelastic damping materials over the ABH portion has been shown to be necessary to draw energy away from the system [1], a

phenomenon which was later confirmed in other works [3, 5-7]. Therefore, the use of the damping layers constitutes an indispensable part in the realization of the ABH effect.

However, it was also observed that an excessive use of the damping layers could cause adverse effects. For example, it was noted that the coating layer may generate non-negligible added stiffness effect to the host structure [7], which in turn would affect the expected ABH effect. Meanwhile, the intuitive way of coating the center of the indentation in an imperfect ABH plate with a modified ABH thickness profile would increase its minimum thickness and then offset the focal point of energy localization [8]. Using a laser excitation and wave decomposition technique, the existence of an optimal thickness for the damping layer which leads to minimum wave reflections was experimentally determined. It was observed that the excessive use of the coating may compromise or even jeopardize the expected energy focalization due to its dynamic interference with the host structure, leading to an impaired energy dissipation [9]. More recently, it was discovered that the use of damping layers could also increase the sound radiation efficiency of an ABH panel due to the additional stiffness effect [10]. All these observations point at the need for a meticulous design and optimization of the layout of the damping layers in order to strike a balance between their dual effects: damping enhancement and stiffness-induced increase in the wave reflection and sound radiation efficiency. However, systematic investigations of the issue, as well as the development of the required topological optimization tools, are still lacking.

Topological optimization of sound radiation requires the provision of two major components: an efficient vibro-acoustic solver and an adaptive optimizer. For the former, numerical methods such as Finite Element Method (FEM) and Boundary Element Method (BEM) have long been

recognized as the most versatile tools to deal with various types of ABH problems [5, 11, 12]. FEM/BEM discretizes the solution domain into meshes, a process that needs to be repeated in every optimization loop, which is very computationally intensive and cumbersome. In that regard, our previously developed semi-analytical sound radiation model [10] shows its advantages. Combining Daubechies Wavelet (DW) scaling functions as the admissible functions under Rayleigh-Ritz framework and Rayleigh integral for sound radiation, that model provides an ideal platform to incorporate the add-on damping layers and accommodate the changing topology incurred during the optimization process. In fact, due to the energy-based and modular nature of the model, the coating area to be optimized can be discretized into a number of elementary sections. Employing the Solid Isotropic Material with Penalization (SIMP) method [13], the stiffness and mass matrices for each section, and the complex normal velocity of the plate are readily available for sensitivity analysis of the objective function with respect to design variables.

As another important component, structural topology optimization has been widely studied for various vibration problems such as the optimization of fundamental eigen-frequencies [14-16], band gaps [17, 18], system loss factors [19] and dynamic compliance [20] etc. Minimization of structural vibrations [21-24] and their sound radiation under harmonic excitations is another important topic for topology optimization. So far, much work has focused on the topology optimization of structures to achieve better acoustical properties. Using a mixed finite element formulation, Yoon *et al.* [25] minimized the averaged sound pressure of 2D vibro-acoustic structures within a frequency interval. Du and Olhoff [26] topologically optimized vibrating bi-material structures to minimize their radiated sound power. Meanwhile, optimization of damping layers to minimize vibration response and sound radiation has also attracted the attention of many researchers. Employing the complex mode superposition method, damping

layers in shell structures were optimized to minimize the vibration amplitude at specific points [22, 27]. Zhang and Kang [28] also optimized the layout of damping layers in a square plate and a hollow box to achieve minimized sound pressure at specific points under harmonic excitations.

So far, topological optimization design of ABH structures for sound radiation minimization has not been dealt with in the literature. The only remotely related paper is the one by Rothe *et al.* [29], in which the position of acoustic black holes was optimized for sound radiation of ABH plates using evolutionary optimization algorithm. As previously discussed, damping layer plays an important role in achieving ABH effect for the mitigation of vibration and sound radiation. Considering the dual conflicting effects of the damping layers, *e.g.* enhancing system damping and increasing its sound radiation efficiency [10], and the lack of analysis and understanding on the topic, we explore the issue in this paper by proposing a general methodology for the topological optimization of the layout of damping layers on an acoustic black hole (ABH) plate. By combining the previous semi-analytical wavelet plate model, the Solid Isotropic Material with Penalization method (SIMP) and the Optimality Criteria (OC) method [30], the sound radiation into a free space by ABH plates is minimized at either a given frequency or within a frequency band.

The paper is organized as follows. Section 2 recalls the semi-analytical wavelet model and describes the formulation of the topology optimization. As an important component in the optimization process, a sensitivity analysis of the objective function with respect to design variables is derived using adjoint variable method (AVM), under the wavelet framework. Numerical results and analyses are presented in Section 3. Main focus is put on the minimization of the radiated sound power of ABH plates. Effects of damping layers deposited at the central

area of the ABH indentation are first analyzed. With the same amount of damping material, optimal placement of the damping layers is then topologically searched at a given frequency or within a frequency band. For comparison, minimization of the mean square velocity of the plates is also conducted. Wavenumber analyses are performed on different configurations to illustrate the underlying physical process as a result of the optimization. Finally, conclusions are drawn in Section 4.

2. Theory

2.1 2D semi-analytical model

The physical system under the investigation is shown in Fig. 1. It consists of a plate (with a lateral dimension of a, b) containing a circular ABH indentation, and symmetrically coated on both sides by damping layers of arbitrary shape. The circular ABH indentation has a radius of R_{ABH} , centered at (x_c, y_c) . The thickness of the uniform part of the plate is h , while that of the circular ABH indentation follows $h(x, y) = \varepsilon \left(\sqrt{(x-x_c)^2 + (y-y_c)^2} \right)^\gamma + h_0$, where ε is a constant, γ the power law index, and h_0 the smallest thickness of the indentation, referred to as the truncation thickness. Uniformly distributed artificial springs, in both translation and rotation with adjustable spring constants, are used along the edges of the plate to simulate different boundary conditions. The plate is excited by a harmonic point force excitation. We are interested in both the plate vibration and its sound radiation into a free and baffled half-space. The previously developed semi-analytical modeling procedure [3] is briefly recalled for the sake of completeness. The model will later be used for topology optimization.

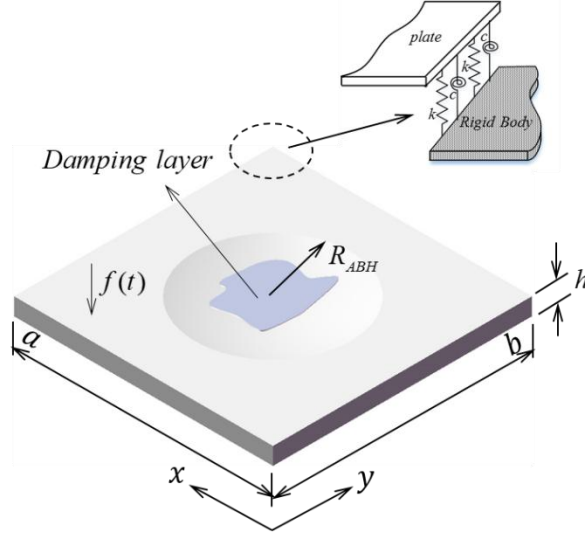


Fig. 1. Modelling of the ABH plate.

For plate modelling, Rayleigh-Ritz framework is followed, based on the Love-Kirchhoff thin plate theory. More specifically, the displacement field of the system can be described as

$$\{u, v, w\} = \left\{ -z \frac{\partial w}{\partial x}, -z \frac{\partial w}{\partial y}, w \right\} \quad (1)$$

where vector $\{u, v, w\}$ contains the displacements of a point in either the plate or the damping layer in three directions. For the convenience of the optimization (to be detailed later), damping layers will be segmented into small sections/elements. It is easy to observe that the above displacement description exhibits a nice additive property to automatically ensure the compatibility and the deformation continuity (in both displacement and rotation) of any two adjacent damping pieces along their junction.

The transverse displacement w is decomposed over a set of assumed admissible functions. In the dimensionless coordinates $\bar{x} = x/a$ and $\bar{y} = y/b$, w can be expressed as

$$w = \sum_{i=1}^{\bar{p}} \sum_{j=1}^{\bar{q}} a_{ij}(t) \varphi_i(\bar{x}) \varphi_j(\bar{y}) \quad (2)$$

in which $\varphi_i(\bar{x})$ and $\varphi_j(\bar{y})$ are the admissible functions; \bar{p} and \bar{q} are the truncation orders

and $a_{ij}(t)$ are complex coefficients to be determined. In the present case, Daubechies wavelet (DW) scaling functions are used as the admissible functions. The properties of the DW functions as well as the selection of \bar{p} and \bar{q} are thoroughly discussed in [3]. After expressing various energy and work terms of the system to form the Hamilton's functional, Euler-Lagrange equations are applied, which leads to the following discretized equation of motion, cast into a matrix form as

$$(\mathbf{K} - \omega^2 \mathbf{M}) \mathbf{A} = \mathbf{F} \quad (3)$$

where \mathbf{K} and \mathbf{M} represent the global stiffness and mass matrices, respectively; \mathbf{A} is the amplitude vector containing the generalized displacement unknowns; ω is the circular frequency and \mathbf{F} the amplitude of the excitation force. In the above procedure, complex Young's moduli which include material loss are introduced for different constituents of the plate assembly: $E_0^* = E_0(1 + i\eta_0)$ and $E_d^* = E_d(1 + i\eta_d)$ for the plate and the damping layer, respectively, in which η_0 and η_d are the corresponding loss factors. It is also relevant to note that damping layers are explicitly modeled as an integrate part of the system in a fully coupled manner.

For the sound radiation modeling, the plate is assumed to radiate sound into an infinite free space with a rigid baffle. Using the Rayleigh integral, we obtain the pressure on the surface of the plate

$$p(r_m) = \frac{j\omega\rho_a}{2\pi} \iint_S v(r_n) \frac{\exp(-jkr_{mn})}{r_{mn}} dS \quad (4)$$

in which k is the acoustic wavenumber, ρ_a the density of air, and S the area of vibrating plate.

$r_{mn} = |r_n - r_m|$ is the distance between two arbitrary position vectors r_m and r_n . The sound power radiated into the semi-infinite space is written as

$$W_{rad} = \frac{1}{2} \text{Re} \left[\iint_S p(r_m) v^*(r_m) dS \right] \quad (5)$$

Considering Eq. (4), Eq. (5) can be discretized and written into the following matrix form

$$W_{rad} = \mathbf{V}^H \mathbf{R}_0 \mathbf{V} \quad (6)$$

where \mathbf{V} is the vector containing complex normal velocity terms of the plate, superscript H is the Hermitian transpose operator, and \mathbf{R}_0 the radiation resistance matrix, with details given in [10].

2.2 Formulation of topology optimization

The layout of the damping layers is to be optimized within a pre-defined search/design space, which is divided into a number of elementary sections. Fig. 2 schematically shows an example of the optimized configuration, in which the segmented elements are denoted either by 1 or 0, indicating that the corresponding area is either fully coated or not coated by damping layer, respectively. Note during the optimization process, however, values associated to each element evolve from 0 to 1, before reaching the final optimized configuration, as detailed later.

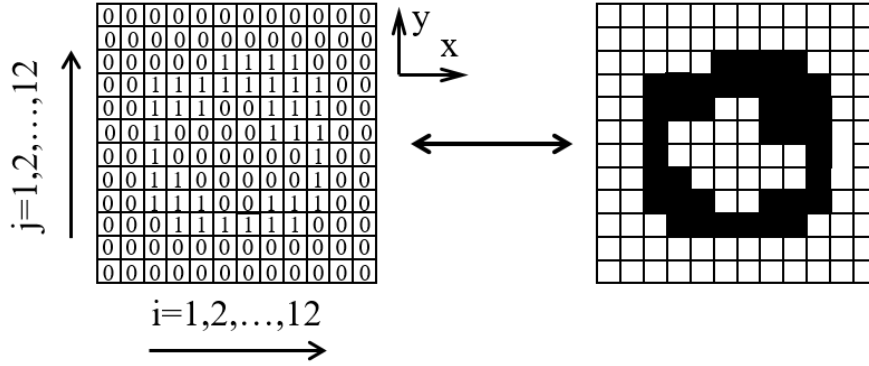


Fig. 2. Optimized layout of damping layers.

The model described in Section 2.1 is used to topologically optimize the layout of a given amount of damping material to minimize various physical quantities such as the plate vibration or the radiated sound power. In the latter case, assuming $\mathbf{S} = \mathbf{K} - \omega^2 \mathbf{M}$, the optimization problem within a frequency band, from f_l to f_u , can be mathematically defined as

$$\min. \quad C = \int_{f_l}^{f_u} \mathbf{V}^H \mathbf{R}_0 \mathbf{V} df \quad (7a)$$

$$\text{s.t.} \quad \mathbf{S}\mathbf{A} = \mathbf{F} \quad (7b)$$

$$\sum_{e=1}^{N_e} \rho_e v_e - f_v \sum_{e=1}^{N_e} v_e \leq 0 \quad (7c)$$

$$0 < \rho_{\min} \leq \rho_e \leq 1 \quad (7d)$$

in which C is the objective function; min. is the abbreviation of *minimize*; and s.t. the abbreviation of *subject to*. The constraint condition Eq. (7c) imposes a restriction on the volume of the damping material used in the optimization process. f_v represents the prescribed volume fraction. N_e is the total number of segmented elements within the design area. v_e is the volume of damping material for element e . Note ρ_e is an important control parameter defining the degree of fulfillment of an element e by the damping material, which can be regarded as a relative density term of the damping layer. The constraint condition Eq. (7d) indicates that the relative density changes within 0 and 1 in the process of iteration. Usually, a lower limit ρ_{\min} , a small positive value, should be assigned in the calculation procedure.

With the aforementioned topology representation, the global stiffness and mass matrices of the system are assembled as

$$\begin{aligned} \mathbf{K} &= \mathbf{K}^{plate} + \sum_{e=1}^{N_e} \mathbf{K}_e^{damp} \\ \mathbf{M} &= \mathbf{M}^{plate} + \sum_{e=1}^{N_e} \mathbf{M}_e^{damp} \end{aligned} \quad (8)$$

where \mathbf{K}^{plate} and \mathbf{M}^{plate} are the stiffness and mass matrices of the base plate respectively; \mathbf{K}_e^{damp} and \mathbf{M}_e^{damp} are those of the damping layers for section e , respectively.

Employing the Solid Isotropic Material with Penalization (SIMP) method [13], \mathbf{K}_e^{damp} and \mathbf{M}_e^{damp} can be expressed as

$$\begin{aligned}\mathbf{K}_e^{damp} &= (\rho_e)^{\tilde{p}} \tilde{\mathbf{K}}_e^{damp} \\ \mathbf{M}_e^{damp} &= (\rho_e)^{\tilde{q}} \tilde{\mathbf{M}}_e^{damp}\end{aligned}\quad (9)$$

in which $\tilde{\mathbf{K}}_e^{damp}$ and $\tilde{\mathbf{M}}_e^{damp}$ are respectively the stiffness and mass matrices for section e when $\rho_e = 1$. \tilde{p} and \tilde{q} are the penal factors that are selected to be 3 in this study.

With given initial values, the design variable ρ_e for each section e will be updated during the optimization process. When the iteration terminates to reach a complete converged result, ρ_e will be either 0 or 1, corresponding to an empty and fully coated element, respectively.

2.3 Sensitivity analysis for optimization

The minimization problem defined in Eqs. (7a)-(7d) requires the calculation of the sensitivity of the objective function C with respect to the design variable ρ_e . The sensitivity of the objective function is derived using adjoint variable method (AVM) [22]. To make the paper self-contained, some key equations related to AVM are recalled from [22], cast into the present modelling framework and briefly presented below. Using Eq. (2), the vector of complex normal velocity can be written as

$$\mathbf{V} = \mathbf{\Phi} \dot{\mathbf{A}} \quad (10)$$

where $\mathbf{\Phi}$ is a matrix composed of wavelet scaling functions [10]. Therefore, C depends on the complex coefficients \mathbf{A} . To derive the sensitivity expression, C is written as:

$$C = C(\mathbf{A}) + \boldsymbol{\mu}_1^T (\mathbf{S}\mathbf{A} - \mathbf{F}) + \boldsymbol{\mu}_2^T (\overline{\mathbf{S}\mathbf{A}} - \overline{\mathbf{F}}) \quad (11)$$

where $\boldsymbol{\mu}_1^T$ and $\boldsymbol{\mu}_2^T$ are the adjoint vectors.

Differentiating Eq. (11) with respect to ρ_e yields

$$\frac{dC}{d\rho_e} = \boldsymbol{\mu}_1^T \frac{\partial \mathbf{S}}{\partial \rho_e} \mathbf{A} + \boldsymbol{\mu}_2^T \frac{\partial \bar{\mathbf{S}}}{\partial \rho_e} \bar{\mathbf{A}} + \left(\frac{\partial C}{\partial \mathbf{A}^R} + \boldsymbol{\mu}_1^T \mathbf{S} + \boldsymbol{\mu}_2^T \bar{\mathbf{S}} \right) \frac{\partial \mathbf{A}^R}{\partial \rho_e} + \left(\frac{\partial C}{\partial \mathbf{A}^I} + i\boldsymbol{\mu}_1^T \mathbf{S} - i\boldsymbol{\mu}_2^T \bar{\mathbf{S}} \right) \frac{\partial \mathbf{A}^I}{\partial \rho_e} \quad (12)$$

Assuming

$$\boldsymbol{\mu}_1^T \mathbf{S} = -\frac{1}{2} \left(\frac{\partial C}{\partial \mathbf{A}^R} - i \frac{\partial C}{\partial \mathbf{A}^I} \right) \quad (13)$$

and $\boldsymbol{\mu}_2^T = \boldsymbol{\mu}_1^T$, where i is the imaginary unit, Eq. (12) can be written as

$$\frac{dC}{d\rho_e} = 2 \operatorname{Re} \left(\boldsymbol{\mu}_1^T \frac{\partial \mathbf{S}}{\partial \rho_e} \mathbf{A} \right) \quad (14)$$

Discretizing the integration in Eq. (7a) and considering Eq. (10) yield

$$\begin{aligned} \frac{\partial C}{\partial \mathbf{A}^R} &= \omega^2 \sum_{i=1}^N \frac{\partial C}{\partial \mathbf{W}_i^R} \frac{\partial \mathbf{W}_i^R}{\partial \mathbf{A}^R} = 2\omega^2 \mathbf{W}_R^T \mathbf{R}_0 \boldsymbol{\Phi} \\ \frac{\partial C}{\partial \mathbf{A}^I} &= \omega^2 \sum_{i=1}^N \frac{\partial C}{\partial \mathbf{W}_i^I} \frac{\partial \mathbf{W}_i^I}{\partial \mathbf{A}^I} = 2\omega^2 \mathbf{W}_I^T \mathbf{R}_0 \boldsymbol{\Phi} \end{aligned} \quad (15)$$

where \mathbf{W} is the complex displacement vector of the plate with subscripts R and I indicating the real part and imaginary part, respectively. N is the number of vibrating points on the investigated system. Substituting Eq. (13) and Eq. (15) into Eq. (14) yields

$$\begin{aligned} \frac{dC}{d\rho_e} &= 2 \operatorname{Re} \left(\boldsymbol{\mu}_1^T \frac{\partial \mathbf{S}}{\partial \rho_e} \mathbf{A} \right) \\ &= -2 \sum_{j=1}^J \omega_j^2 \operatorname{Re} \left(\mathbf{W}^H \mathbf{R}_0 \boldsymbol{\Phi} \mathbf{S}^{-1} \frac{\partial \mathbf{S}}{\partial \rho_e} \mathbf{A} \right) \Delta f \end{aligned} \quad (16)$$

in which J is the number of discretized frequencies. Optimizations at a single frequency can be treated as a special case of the above defined optimization problem. In that case, Eq. (16) degenerates to

$$\frac{dC}{d\rho_e} = -2\omega^2 \operatorname{Re} \left(\mathbf{W}^H \mathbf{R}_0 \boldsymbol{\Phi} \mathbf{S}^{-1} \frac{\partial \mathbf{S}}{\partial \rho_e} \mathbf{A} \right) \quad (17)$$

Meanwhile, if the focus is on the minimization of the plate vibrational response in terms of

mean square velocity, a parallel formulation can be easily established by following the same procedure. In that case, Eq. (16) and Eq. (17) still hold by simply replacing the radiation resistance matrix \mathbf{R}_0 by a unit matrix. Using the above sensitivity expressions, the relative density ρ_e for each section e is updated using an optimizer based on Optimality Criteria (OC) method [30] by

$$\rho_e^{\delta+1} = \left(B_e^\delta\right)^\zeta \rho_e^\delta \quad (18)$$

where δ is the number of iteration; ζ the numerical damping coefficient [30] and $B_e^\delta = \max\left(0, -(dC/d\rho_e)/\lambda\right)$, where λ is a Lagrangian multiplier which can be obtained using bi-sectioning algorithm. During the process of iteration, a mesh-independency filter [31] is used to avoid the checkboard pattern.

2.4 Validation examples

The proposed topology optimization procedure involves two modules: a numerical solver of the physical system (vibration and sound radiation model) and an optimizer. The former has been thoroughly validated in a previous work [10], in terms of both vibration and sound radiation prediction. Hereafter, the optimizer is to be validated. To that end, the test case used in [22] is considered, in which damping layers coated on a simply supported square plate are topologically optimized. The plate is made of aluminum and has a dimension of $3 \times 3 \times 0.02$ m. Using the same set of geometrical and material parameters, the current model differs slightly from [22] in two aspects: 1) a structural damping model via complex Young's modulus is used for the damping layer in the present model, instead of a Rayleigh damping model used in [22]; 2) the plate is symmetrically covered on both sides in the current model, whilst in Ref. [22], the same amount of damping was applied on only one side of the plate.

The damping layers are discretized into 30×30 meshes, in contrast to 60×60 meshes

used in the Ref. [22]. Same as in [22], a point force excitation is applied at the center of the plate. The square of the amplitude of vibration displacement at the excitation point is chosen as the objective function. The iteration process terminates when the convergence criteria $\left(\left|\rho_e^{\delta+1} - \rho_e^{\delta}\right|/\rho_e^{\delta}\right)_{\max} < 0.01\%$ is satisfied. Using the optimization method described in Sections 2.2 and 2.3, the resulting optimal damping layout is compared with the results given in [22] using mathematical programming algorithm (MMA). Among several frequencies being tested, three typical ones are shown in Fig. 3 for $f = 30, 60, 90$ Hz, respectively. It can be seen that both set of results agree in terms of coverage topology. The present model uses a smaller number of elements which inevitably affects the resolution of the image. Meanwhile the aforementioned differences in the model also contribute to the observed differences. Nevertheless, the proposed optimization algorithm gives the optimized configurations, consistent with results from [22], thus validating the established optimization approach.

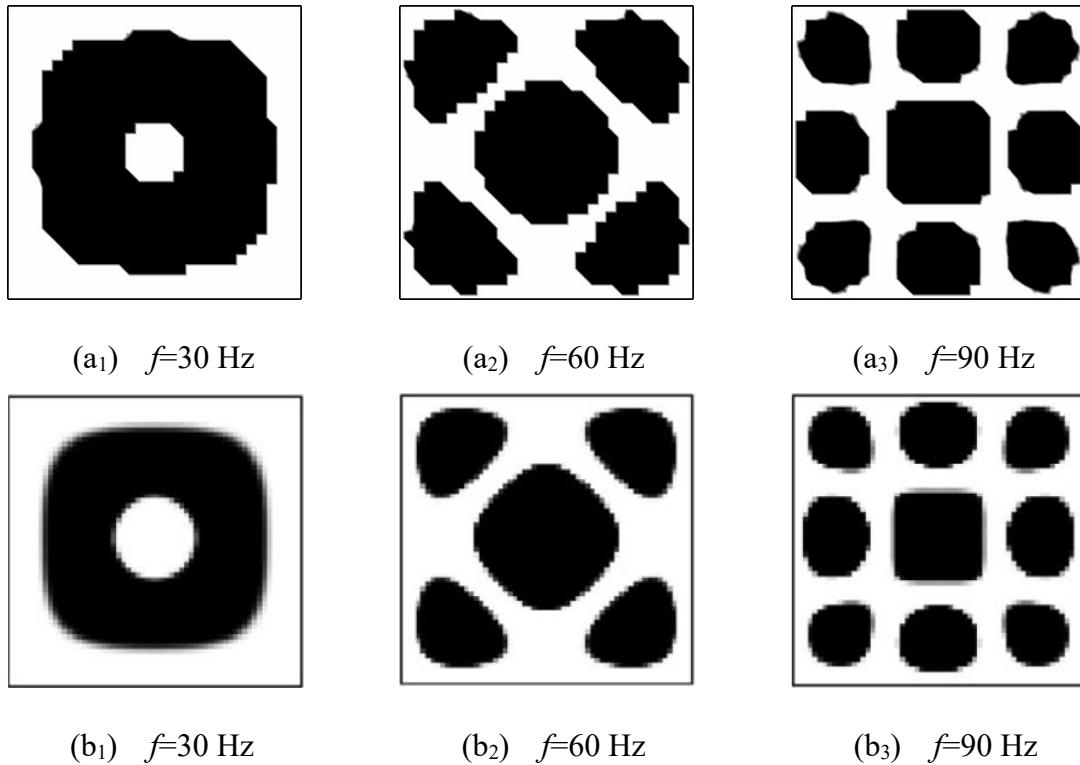


Fig. 3. Optimal layout of damping layers at different frequencies: Present model with OC method (a₁-a₂-a₃);

3. Numerical analyses

Numerical examples and analyses use a simply-supported ABH plate with geometrical and material parameters tabulated in Table 1. Apart from those previously defined parameters, additional ones include the densities ρ_0 , ρ_d and Poisson's ratios ν_0 , ν_d for the plate and the damping layers, respectively. The reference case is defined as the one with central part of the ABH indentation fully coated inside a circle with a radius of $R_d = 86.5$ mm. In this reference case, referred to as circular case hereafter, the damping layer has a uniform thickness $h_d = 0.3$ mm on each side of the plate. The basic sound radiation phenomena of this reference case, in particular the effect of the damping layers, will first be illustrated. Then, topological optimization will be applied to determine the optimal coating layout which allows the minimization of the radiated sound power, by using the same amount of damping material, at either a given frequency or within a pre-defined frequency band. A harmonic point force is applied at (0.05, 0.315) m over the uniform portion.

Table 1 – Geometrical and material parameters

Geometry		Material	
$a=0.5$ m	$x_c=0.25$ m	$E_0=200$ GPa	$E_d=5$ GPa
$b=0.45$ m	$y_c=0.25$ m	$\nu_0=0.3$	$\nu_d=0.3$
$h=4.7$ mm	$\varepsilon=0.2$ /m	$\eta_0=0.01$	$\eta_d=0.3$
$R_{ABH}=0.15$ m	$\gamma=2$	$\rho_0=7800$ kg/m ³	$\rho_d=950$ kg/m ³
$h_0=0.2$ mm	$h_d=0.3$ mm		

3.1 Effect of damping layers on the vibration and sound radiation of ABH plates

Using the previously developed DW model, the effect of the damping layers (reference case with central circular coating) on the vibration of the ABH plates and their radiated sound field are first analyzed to show the necessity of the optimization. A bare ABH plate without any damping treatment is taken as comparison basis. Similar comparisons were reported in Ref. [10]. For the completeness of this paper, however, some important comparative results between the ABH plates with/without central circular coating are recapped here, as shown in Fig. 4. Figs. 4(a) and (b) show the comparisons in terms of the radiated sound power level and the corresponding mean square velocity level (referenced to $1 \text{ m}^2/\text{s}^2$) of the plates, averaged over their entire surface. It can be seen that, compared with the bare plate, the use of the damping layers obviously reduces the resonance peaks as well as the overall level of the both the plate vibration level and the radiated sound power, especially above the cut-on frequency [5]. The so-called cut-on frequency

is an indicative frequency defined as $f_{cut-on} = \frac{\pi h}{2(R_{ABH})^2} \sqrt{\frac{E_0}{12\rho_0(1-\nu_0^2)}}$ at which the wavelength

of the incident bending waves start to be equal to the characteristic dimension (the diameter of the circular indentation in the present case) of the ABH indentation. It is commonly accepted that the bending waves interact more effectively with the ABH indentation above this frequency, thus producing systematic ABH effects. In the present case, the cut-on frequency is 500 Hz. Above the cut-on frequency, these aforementioned phenomena are obviously due to the coating-enhanced ABH effects in terms of energy focalization and dissipation towards the indentation center. A less known phenomenon, however, is the coating-induced changes in the sound radiation efficiency of the plate as shown in Fig. 4(c). In fact, the deployment of the damping layers generates an obvious increase in the sound radiation efficiency of the plate, again

more obvious and systematic after the ABH cut-on. The increase in the radiation efficiency is attributed to the additional stiffness of the damping layers rather than their mass, as demonstrated in Ref. [10]. The trend continues even after the critical frequency of the plate calculated based on

the thickness of the uniform portion of the plate by $f_{critical} = \frac{c_a^2}{2\pi} \sqrt{\frac{12\rho_0(1-\mu_0^2)}{E_0h^2}}$. Above $f_{critical}$,

the length of the bending waves inside the plate becomes larger than that of the acoustic waves.

In another word, structural waves travel faster than their acoustic counterparts, thus producing the so-called supersonic structural waves, which are shown to be efficient in sound radiation by classical structural acoustic theory. Thanks to the gradually decreased thickness of the ABH

indentation, at a given frequency above $f_{critical}$, a so-called transonic circular boundary with a

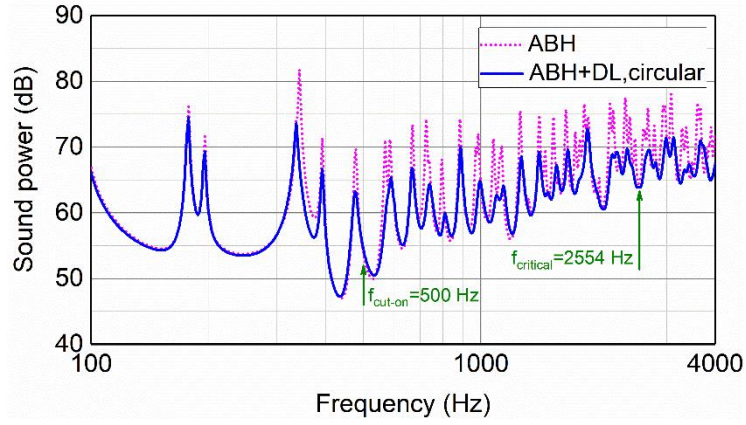
radius of $R_t = \left(c_a^2 \sqrt{12\rho_0(1-\mu_0^2)}/E_0 / (2\pi f \varepsilon) \right)^{1/2}$ is created, which demarcates a subsonic region

inside the circle with a supersonic region outside. Therefore, the inside region within R_t is less

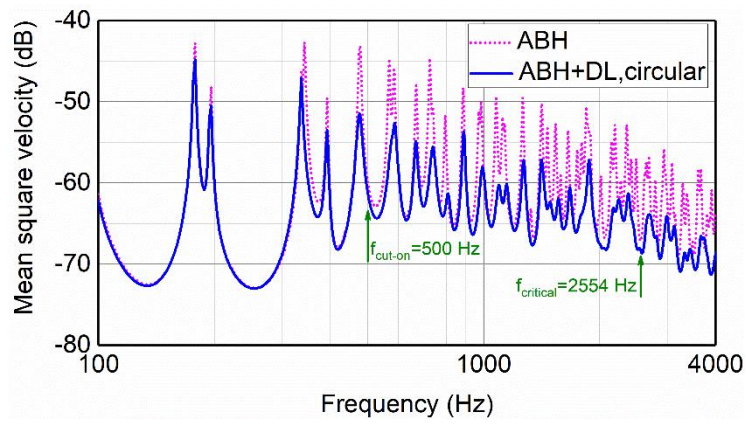
efficient in sound radiation. These observations point at the need for a meticulous design and

optimization of the layout of the damping layers in order to strike a balance between their dual

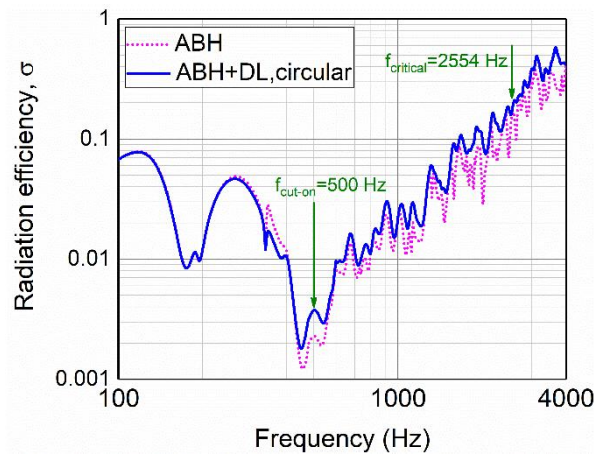
effects: damping enhancement and stiffness-induced increase in the sound radiation efficiency.



(a)



(b)



(c)

Fig. 4. Comparison between ABH plate (dot line) and ABH plate with damping layers (solid line): (a) Radiated sound power; (b) Mean square velocity; (c) Radiation efficiency. DL denotes damping layer.

3.2 Topology optimization for the minimization of sound power

The optimization method is employed to seek solutions to the minimization of the radiated sound power of a plate defined in Section 2 at single frequencies. The design area is a square which frames the ABH external peripheral circle and is discretized into 12×12 elements. The volume fraction f_v is restricted to 0.2618 to make sure that the total volume of damping layer is the same as the reference case with a circular coverage, as discussed in Section 3.1.

An arbitrary frequency of 3480 Hz is chosen to show the typical evolution of the objective function (the radiated sound power level in the present case) during the iteration process in Fig. 5. It can be seen that the objective function undergoes a continuous decrease from 67.1 dB to approach a converged value of 64.9 dB after roughly 10 iterations. Meanwhile, the layout of the damping layer also evolves accordingly, starting from the initial uniform coverage to gradually converge to a stable and fully converged optimal configuration. The grey color shown in the map of configuration of damping layers at step 1 indicates that, at the beginning of iteration, the relative density, ρ_e , is quite different from either 0 or 1. With the increase of iteration loop, ρ_e gradually gets closer to 0 or 1. It is interesting to note that, at this particular frequency, the initially covered central area of the ABH indentation (step 4) tends to be gradually emptied, until reaching the final optimal layout in which the central portion of ABH indentation is not fully coated (steps 9-18), in contrast to the intuitive guess that one might have to simply cover the central area.

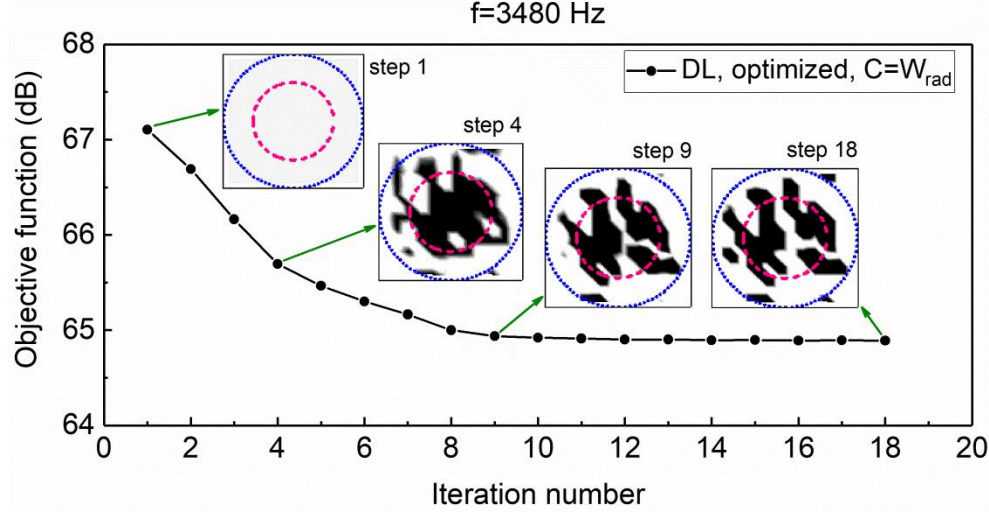
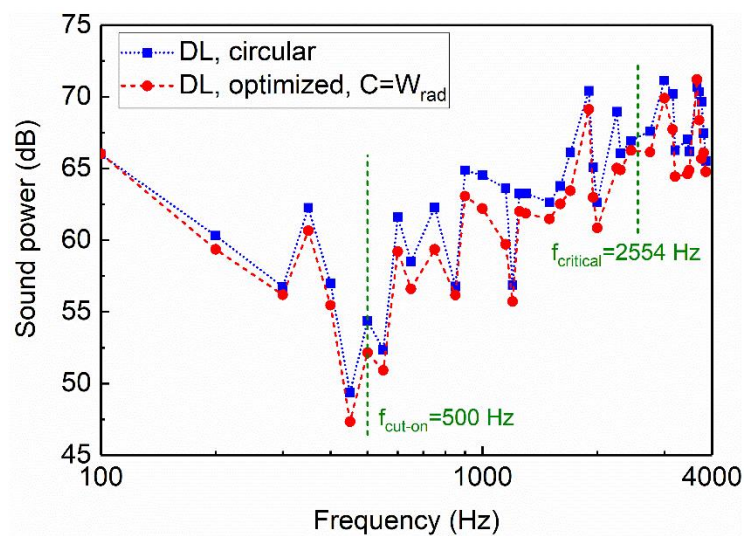


Fig. 5. Convergence of iteration process at $f = 3480$ Hz. The outer dot circle represents the ABH peripheral circle, and the inner dash circle represents the circular coverage of damping layers. DL denotes damping layer and W the radiated sound power. Step 1 is the initial starting configuration.

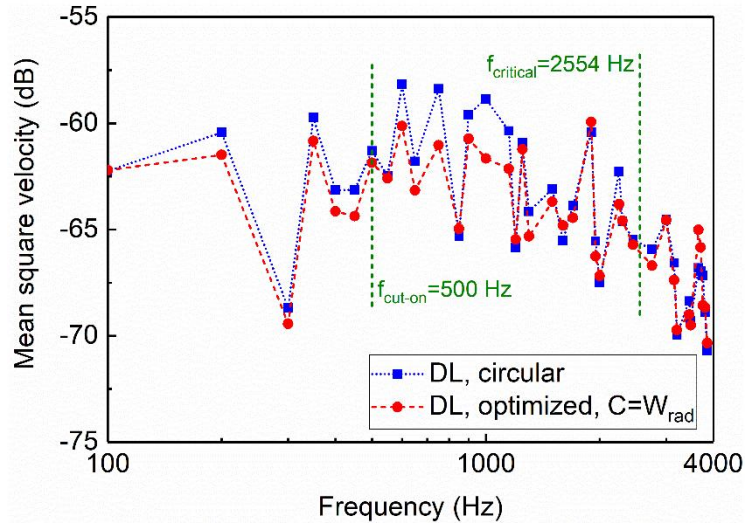
The same process can be followed for every given frequency of interest. The outcome of the optimization is shown in Figs. 6(a)-(c) in terms of sound power level, mean square velocity level as well as the sound radiation efficiency, respectively. Again, results are compared with their reference counterparts with the circular coating using the same amount of damping materials.

Fig. 6(a) shows that, compared with the circular case, the optimal damping layout results in a reduced radiated sound power of different level, which may go up to roughly 4 dB in the present case. Below the cut-on frequency (500 Hz), the effect of the optimization is trivial. The same observation also applies to the mean square velocity of the plate (Fig. 6(b)), as well as the sound radiation efficiency (Fig. 6(c)). This is understandable since ABH effect is absent in this low frequency range so that the room for optimization is basically non-existent. In fact, as to be demonstrated later on, the finally reached optimized layout in the low-frequency range is basically the same as the central coverage case. Above the cut-on frequency, a systematic

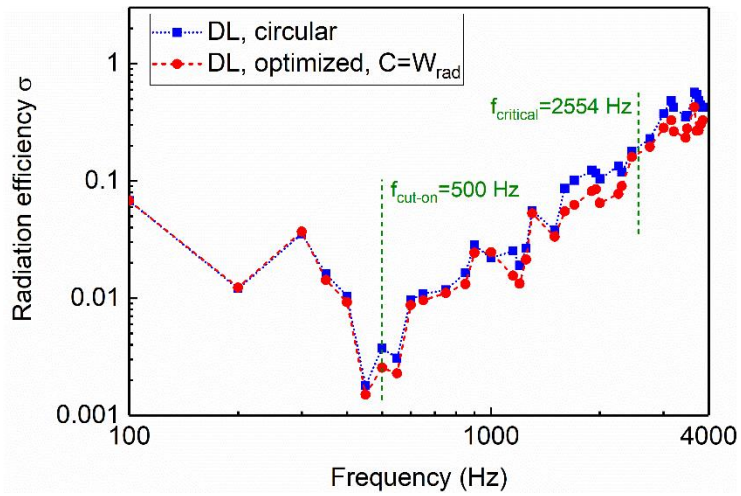
reduction in the radiated sound power starts to show as a result of the optimization. The mean square velocity level, however, though generally following the same reduction trend but to a less degree, exhibits an increase at some frequencies. Note that when approaching and exceeding the critical frequency (2554 Hz), changes in the vibration level becomes even smaller. The above observation suggests that the observed systematic reduction in the sound radiation cannot be totally attributed to the changes in the vibration level of the system. Instead, a possible change in the sound radiation properties of the structure due to the different coating layouts is expected. This is further confirmed by examining the corresponding changes in the sound radiation efficiency of the plate before and after optimization, as shown in Fig. 6(c). It can be seen that, though not being directly used as the objective function, the sound radiation efficiency of the plate is almost systematically reduced by the optimization, more significantly at higher frequencies. This shows that the optimization impacts on the physical system in a way that its sound radiation properties are altered through a more reasonable design of the damping layer layout.



(a)



(b)



(c)

Fig. 6. Comparison between initial case (square symbol) and the case of optimized sound power (circular symbol) at single frequencies: (a) Sound power; (b) Mean square velocity; (c) Radiation efficiency. DL denotes damping layer, and W the radiated sound power.

Meanwhile, the reduction in the radiation efficiency indicates that the plate is less effective in radiating sound. To better show the underlying physical process, a wavenumber transform analysis [32] is performed on the vibration velocity field of the ABH plates at 3480 Hz, with the circular and the optimized damping layout, respectively. To this end, the vibration velocity is transformed from spatial domain to wavenumber domain as:

$$\mathbf{V}(k_x, k_y, f) = \iint \mathbf{V}(x, y, f) e^{-j(k_x x + k_y y)} dx dy \quad (19)$$

where k_x and k_y are the wavenumbers in x and y directions, respectively, and $\mathbf{V}(k_x, k_y, f)$ is the vibration velocity in wavenumber domain. Fig.7 shows a plot of the two normalized wavenumber components \bar{k}_x and \bar{k}_y of $\mathbf{V}(k_x, k_y, f)$, i.e., k_x and k_y are normalized with respect to $k = 2\pi f/c_a$, where c_a is the speed of sound. The circle on each figure denotes a unit radiation circle which demarcates the vibrational supersonic components of the plates (inside the circle) from the subsonic ones (outside the circle).

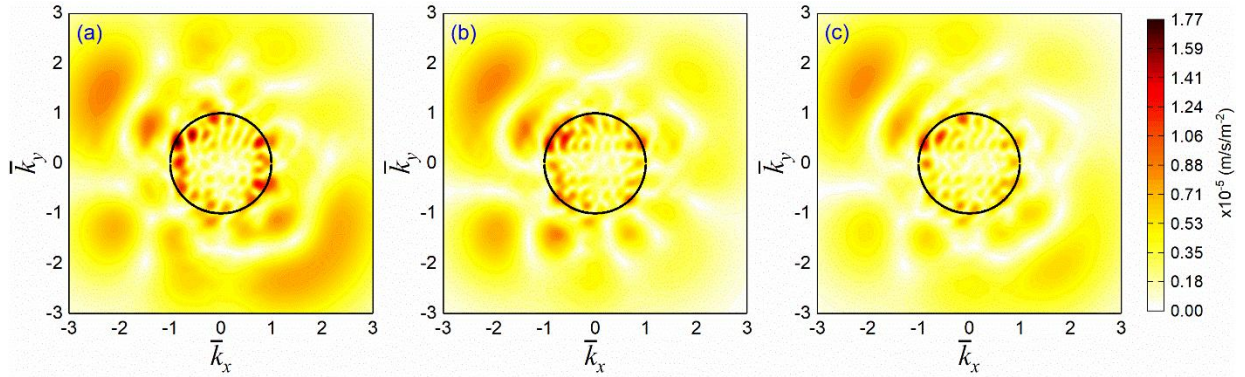


Fig. 7. Wavenumber spectra of ABH plates at 3480 Hz: (a) ABH plate with no damping layers; (b) ABH plate with damping layers coated inside a central circle; (c) ABH plate with optimized damping layers. The solid circle indicates the normalized radiation circle with radius of $r=1$.

It can be seen from Fig. 7 that for the bare plate (Fig. 7(a)), energetic vibration components

are mainly located inside the radiation circle. This is understandable since the frequency under investigation is above the critical frequency of the flat plate; therefore, supersonic components exist in the system. With circular damping coverage (Fig. 7(b)), supersonic components inside the radiation circle is reduced. This trend is further accentuated with the optimal damping layout, as shown in Fig. 7(c). Therefore, the wavenumber analysis further confirms the fact that the optimal layout of the damping layer changes the sound radiation properties of the plate by reducing the supersonic components in the plate vibration, thus resulting in a minimized radiated sound power.

3.3 *Vibration minimization Vs. sound radiation minimization*

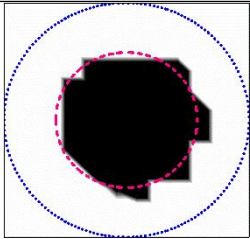
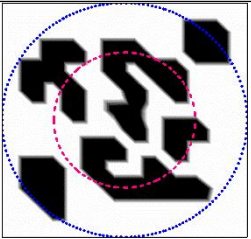
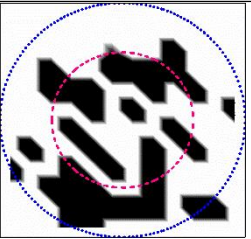
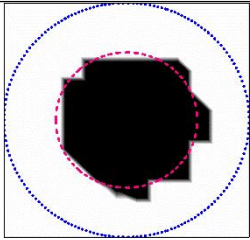
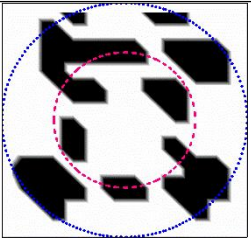
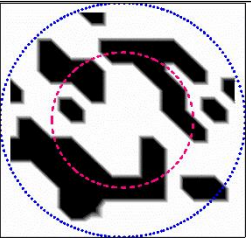
The previously established optimization methodology applies to the optimization of both sound radiation and structural vibration. Since the excessive use of the damping layer may affect both the wave reflection and sound radiation, probably in different ways, it is relevant to examine the issue to understand its impact on the final optimized system topology. To this end, the optimal damping layer layouts based on vibration minimization (using the mean square velocity, MSV, of the plate) and sound radiation minimization (using radiated sound power, W_{rad}) are compared at three representative frequencies: 100 Hz (before the ABH cut-on), 1700 Hz (after cut-on) and 3150 Hz (above the critical frequency). Results are tabulated in Table 2 for comparisons. It can be seen that, at the low-frequency of 100 Hz, which is below the cut-on frequency and around the first natural frequency (92 Hz) of the plate, both optimization problems lead to basically the same optimal damping layout with a central coverage. With the increase of frequency (above the ABH cut-on), differences between the two cases start to be noticeable. Specifically, compared with the structural vibration minimization, optimized coated area based on sound radiation tends to be further away from the central portion of the ABH indentation. This is an indication that the

adverse effect of the coating, which is presumably more significant at the ABH center, is more significant on sound radiation (e.g. increased sound radiation efficiency) than on structural vibration (increased wave reflections). To quantify this phenomenon and also to examine its applicability to other frequencies, a Coverage Ratio (CR) is used to quantify the fulfillment level of the central area of the ABH indentation. CR is defined as the ratio between the coated area inside the inner dash circle depicted in Table 2 (corresponding to the periphery of the circular coverage) and the total area inside the circle.

CR curves for both the MSV and W_{rad} optimization within the entire frequency range of interest are compared in Fig. 8. It shows that, with only a few exceptions, CR based on W_{rad} optimization is smaller than its MSV-based counterpart at almost all frequencies, especially above the ABH cut-on frequency. This confirms the general character of the optimal damping layout observed before.

As can be seen from Table 2, in contrast to the vibration optimization, damping layers tend to spread more towards the periphery region of the ABH indentation as a result of acoustic optimization. This is understandable since, as shown in Fig. 6(c), damping layers coated at the central portion of the ABH indentation (with very thin thickness and therefore weak stiffness) would increase the radiation efficiency of the structure. This observation further confirms the fact that, among the dual adverse effect of the damping in terms of the increased wave reflection and radiation efficiency, the latter seems to be more dominant. While the vibration optimization only needs to cope with the former, acoustic optimization has to deal with both. Therefore, through the optimized damping layout, the acoustic benefit is achieved as a result of balanced consideration of both aspects, predominantly through a reduced radiation efficiency.

Table 2 – Comparison of optimal layouts of damping layers under different objective functions. The outer dot circle represents the ABH peripheral circle, and the inner dash circle represents the circular coverage of damping layers.

Optimal layout	$f = 100$ Hz	$f = 1700$ Hz	$f = 3150$ Hz
Objective function, C , is taken as the mean square velocity of the plate, MSV.			
Objective function, C , is taken as the radiated sound power, W_{rad} .			

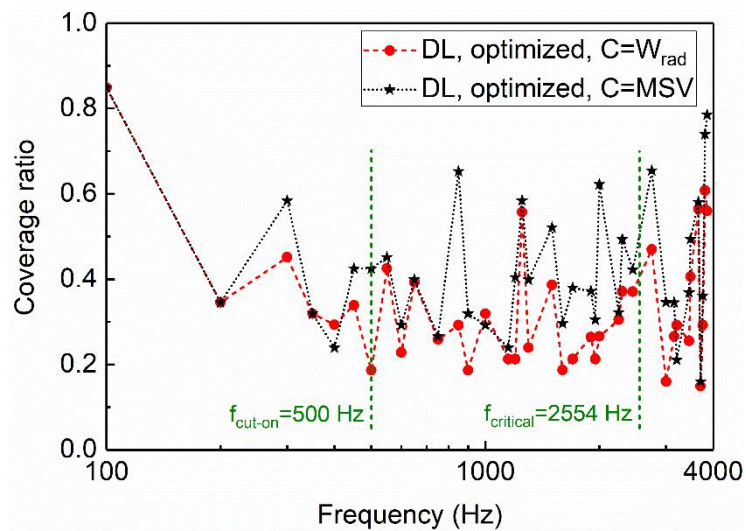


Fig. 8. Comparison of the coverage ratios. W_{rad} : Sound power optimization (circular dot); MSV: mean square velocity optimization (star dot).

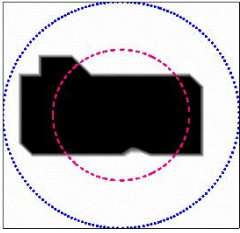
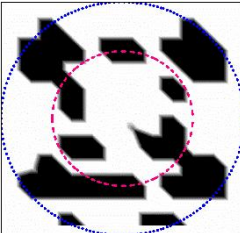
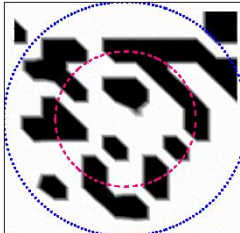
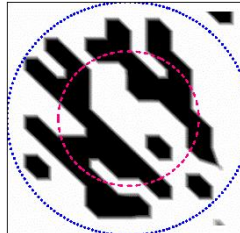
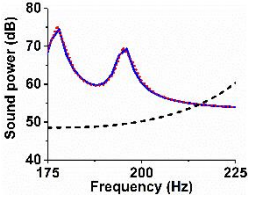
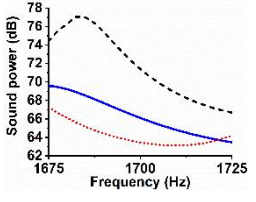
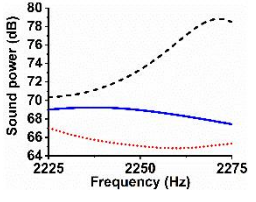
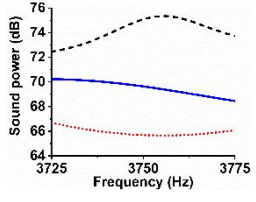
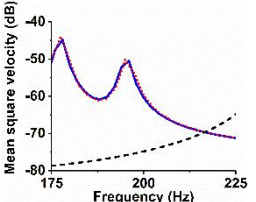
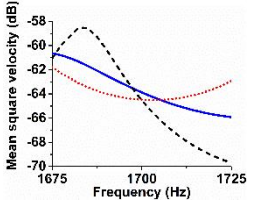
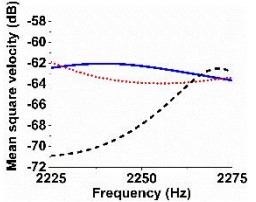
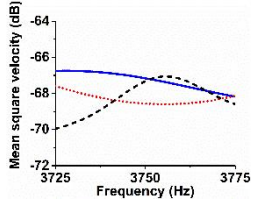
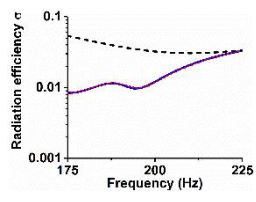
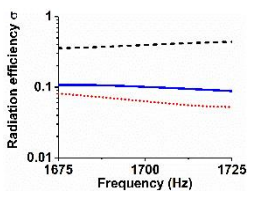
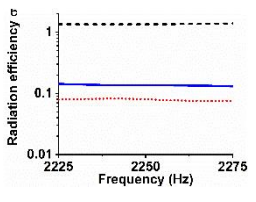
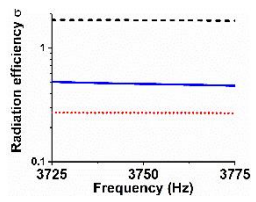
3.4 Minimization of sound power within a frequency band

Possible variations in the excitation frequencies can be dealt with by considering a frequency band instead of discrete frequencies. To investigate the issue, minimizations of the radiated sound power within a prescribed frequency band, mathematically defined in Eqs. (7a)-(7d), is investigated. To this end, an arbitrary frequency band of 50 Hz is chosen as an example. It should be noted that the proposed methodology and tools can be applied to any frequency range. The reason why we choose a 50Hz band is to accommodate a typical engineering scenario in which relatively stable excitation is exerted onto the structure, but with slight variations. Four representative frequency bands are selected for analyses: one below cut-on frequency (175-225 Hz), two between the cut-on frequency and the critical frequency (1675-1725 Hz and 2225-2275 Hz, respectively), and the third one above the critical frequency (3725-3775 Hz). For comparison purposes, central circular coverage configuration is taken as reference to quantify the changes in various physical parameters: sound power variation as well as the overall reduction within the band, alongside the corresponding mean square velocity and the radiation efficiency of the plate. Results are shown in Table 3. The optimal coating layouts for each frequency bands are also presented.

This comparison allows to revisit and confirm the general character of several observations that are previously made using particular discrete frequencies. Again, optimizations allow to determine the optimal layout towards the minimization of the structural sound radiation for any given frequency band. The reduction level resulting from the optimal layout, as compared to the central coverage case using the same amount of damping materials, varies depending on the frequency band of interest, trivial in the non-dynamic low frequency range, and more appreciable

at higher frequencies after the ABH effect is cut-on. Effect of the optimization is quasi-unobservable on any physical parameters of the system at the low frequency, typically below the ABH cut-on. When frequency increases, however, the reduction in the radiated sound power does not always go hand in hand with the variation in the vibration level of the plate. A typical example is the case corresponding to the B-column of Table 3, where vibration level of the plate increases while the radiated sound is reduced within a portion of the frequency band. Having said that, a remarkably consistent phenomenon is that, in all cases considered in Table 3, the sound radiation efficiency of the plate with optimal damping layout is systematically reduced above the ABH cut-on. This further consolidates the conclusion that the reduced sound radiation of the optimized ABH plate roots in an improved sound radiation properties of the structure as a result of the optimization. Meanwhile, the optimal damping coverage is not always concentrated on the central ABH indentation area, consistent with the previous observations made on single frequency cases. It is also relevant to compare the coated cases against a bare plate (with corresponding quantities shown by black dotted lines in Table 3). Below the cut-on frequency, the effect of ABH plate on sound power is not obvious as expected, compared with that of a uniform plate. Above the cut-on frequency, however, as can be seen in column B-2, C-2, and D-2, the reduction in the radiated sound power can be up to 8-10 dB.

Table 3 – Characteristics of sound radiation under different frequency bands. Solid line represents the reference circular case, the dot line the optimized case, and the dash line the uniform plate

Frequency band	$f < f_{cut-on}$	$f_{cut-on} < f < f_{critical}$		$f > f_{critical}$
Reduction	$\Delta W = 0$ dB	$\Delta W = 2.31$ dB	$\Delta W = 3.25$ dB	$\Delta W = 3.60$ dB
Distribution	 A-1	 B-1	 C-1	 D-1
Sound power	 A-2	 B-2	 C-2	 D-2
Mean square velocity	 A-3	 B-3	 C-3	 D-3
Radiation efficiency	 A-4	 B-4	 C-4	 D-4

4 Conclusions

A general topological optimization methodology is proposed in this paper to achieve a minimized vibration or sound radiation of an acoustic black hole (ABH) plate through optimizing the layout of the damping layers coated on its surface. The proposed tool encompasses a 2D semi-analytical Daubechies Wavelet (DW) model with an adaptive optimizer based on the Solid Isotropic Material with Penalty (SIMP) method and the Optimality Criteria (OC) method. System optimization can be performed at either a given frequency or within a prescribed frequency band. The work aims at providing a solution to address the conflicting role that damping layers play in a typical ABH structure in terms of energy dissipation versus degraded structural properties. Based on numerical analyses, the main conclusions are summarized as follows.

- 1) The developed DW model is shown to be flexible and versatile to deal with the topological evolutions incurred during the optimization process. Its energy-based, modular and additive properties in relation to the handling of damping layers make it conducive for topological optimizations.
- 2) The optimization allows a reduction of the radiated sound power at either a given frequency or within a prescribed frequency band. For the configuration investigated in the paper, the reduction level can be up to 4 dB compared with its reference plate with standard damping coating at the ABH center using the same amount of materials. At low frequencies before the ABH cut-on, the reduction in the sound radiation is insignificant due to the absence of the ABH effect, while at high frequencies, the optimization warrants a systematic reduction in the sound

radiation efficiency of the plate, which is the dominant factor leading to the reduced sound radiation. Along with this is an impaired energy level of the supersonic vibration components in the plate.

3) The optimal damping layout, irrespective of the minimization parameters (sound power or mean square velocity), is basically the same as the central coverage configuration below the cut-on frequency of the plate. Above the ABH cut-on, however, the two optimization problems end up with different optimal configurations, which shows that the best coating area may not necessarily be the center of the ABH indentation center. The optimized layout based on sound radiation optimization draws damping material further away from the central portion of the ABH indentation, as compared to the vibration-based optimization does. This shows that the adverse effect of the excessive use of the coating impacts more on the sound radiation than structural vibration.

It is relevant to note that the optimization results reported in this paper obviously depend on numerous parameters of the system such as structural details, excitation as well as the frequencies of interest. The focus of the work is placed on 1) showing a general design methodology by providing the necessary tools and 2) revealing the underlying physical changes in the structural properties alongside the topological evolution of the damping treatment. In that sense, striving for the maximum performance was not the main objective of the current work. Should this be the main objective, the proposed methodology could be extended to also consider other factors such as coating with non-uniform thickness or other non-perfect ABH profiles, for which the system is shown to be more sensitive to the deployment of the damping layers [7, 8].

Acknowledgements

The authors thank the support from Research Grant Council of the Hong Kong SAR (PolyU 152017/17E) and National Science Foundation of China (No. 11532006).

Appendix A: Nomenclature

a	Length of the plate
b	Width of the plate
h	Thickness of the uniform portion of the plate
$h(x, y)$	Variable thickness of the ABH portion
ε	A constant defining the thickness profile
γ	Power law index
h_0	Smallest thickness of the ABH indentation
x_c, y_c	Center position of the ABH indentation
R_{ABH}	Radius of the circular indentation
R_t	Radius of the transonic circular boundary
R_d	Radius the coverage of damping layers
h_d	Thickness of damping layers on each side of plate
E_0	Young's modulus of the plate
E_d	Young's modulus of the damping layers
ρ_0	Mass density of the plate
ρ_d	Mass density of the damping layers
η_0	Loss factor of the plate
η_d	Loss factor of the damping layers
ν_0	Poisson's ratio of the plate
ν_d	Poisson's ratio of damping layers
$\{u, v, w\}$	Vector of displacement
\bar{x}, \bar{y}	Dimensionless coordinates in x and y directions
$a_{ij}(t)$	Generalized coordinates
\bar{p}, \bar{q}	Truncation order
$f(t)$	Excitation force
M	Mass matrix
K	Stiffness matrix
F	Amplitude of excitation force
p	Sound pressure
ω	Circular frequency
f_{cut-on}	Cut-on frequency
$f_{critical}$	Critical frequency

ρ_a	Density of air
c_a	Sound speed
k	Acoustic wavenumber
k_x	Acoustic wavenumber in x direction
k_y	Acoustic wavenumber in y direction
\bar{k}_x	Normalized acoustic wavenumber in x direction
\bar{k}_y	Normalized acoustic wavenumber in y direction
S	Area of the vibrating plate
r_{mn}	Distance between two arbitrary position vectors r_m and r_n
W_{rad}	Radiated sound power
Re	Real part
\mathbf{V}	Vector of complex normal velocity
H	Hermitian transpose operator
C	Objective function
f_l, f_u	Lower and upper limit of the integral in objective functions
f_v	Prescribed volume fraction
v_e	Volume of damping material for element e
ρ_e	Relative density (design variable) of damping material for element e
ρ_{\min}	A small positive value of ρ_e
\mathbf{M}_e	Mass matrix of element e
\mathbf{K}_e	Stiffness matrix of element e
$\tilde{\mathbf{M}}_e^{damp}$	Mass matrix of element e when $\rho_e = 1$
$\tilde{\mathbf{K}}_e^{damp}$	Stiffness matrix of element e when $\rho_e = 1$
N_e	Number of sections of damping layers
\tilde{p}, \tilde{q}	Penal factors for matrices of stiffness and mass of damping layers
Φ	A matrix composed of wavelet functions
\mathbf{A}	Complex amplitude of $a_{ij}(t)$
$\boldsymbol{\mu}_1^T, \boldsymbol{\mu}_2^T$	Adjoint vectors
\mathbf{W}	Vector of complex displacement
N	Number of vibrating points
J	Number of discretized frequencies
φ	Daubechies wavelet scaling function
L	Compactly supported length
δ	Number of iteration
ζ	Damping coefficient
λ	Lagrangian multiplier

References

- [1] V. Krylov, F. Tilman, Acoustic ‘black holes’ for flexural waves as effective vibration dampers, *J. Sound Vib.* 274 (2004) 605-619.
- [2] V. V. Krylov, R. Winward, Experimental investigation of the acoustic black hole effect for flexural waves in tapered plates, *J. Sound Vib.* 300 (2007) 43-49.
- [3] L. Ma, S. Zhang, L. Cheng, A 2D Daubechies wavelet model on the vibration of rectangular plates containing strip indentations with a parabolic thickness profile, *J. Sound Vib.* 429 (2018) 130-146.
- [4] E. Bowyer, V. V. Krylov, Experimental study of sound radiation by plates containing circular indentations of power-law profile, *Appl. Acoust.* 88 (2015) 30-37.
- [5] S. C. Conlon, J. B. Fahnlne, F. Semperlotti, Numerical analysis of the vibroacoustic properties of plates with embedded grids of acoustic black holes, *J. Acoust. Soc. Am.* 137 (2015) 447-457.
- [6] D. O’Boy, V. V. Krylov, Vibration of a rectangular plate with a central power-law profiled groove by the Rayleigh–Ritz method, *Appl. Acoust.* 104 (2016) 24-32.
- [7] L. Tang, L. Cheng, H. Ji, J. Qiu, Characterization of acoustic black hole effect using a one-dimensional fully-coupled and wavelet-decomposed semi-analytical model, *J. Sound Vib.* 374 (2016) 172-184.
- [8] W. Huang, H. Ji, J. Qiu, L. Cheng, Wave energy focalization in a plate with imperfect two-dimensional acoustic black hole indentation, *J. Vib. Acoust.* 138 (2016) 061004.
- [9] H. Ji, J. Luo, J. Qiu, L. Cheng, Investigations on flexural wave propagation and attenuation in a modified one-dimensional acoustic black hole using a laser excitation technique, *Mech. Syst. Signal Proc.* 104 (2018) 19-35.
- [10] L. Ma, L. Cheng, Sound radiation and transonic boundaries of a plate with an acoustic black hole, *J. Acoust. Soc. Am.* 145 (2019) 164-172.
- [11] P. A. Feurtado, S. C. Conlon, An experimental investigation of acoustic black hole dynamics at low, mid, and high frequencies, *J. Vib. Acoust.* 138 (2016) 061002.
- [12] L. Zhao, F. Semperlotti, Embedded Acoustic Black Holes for semi-passive broadband vibration attenuation in thin-walled structures, *J. Sound Vib.* 388 (2017) 42-52.
- [13] M. P. Bendsøe, Optimal shape design as a material distribution problem, *Struct. Optim.* 1 (1989) 193-202.
- [14] A. R. Díaz, N. Kikuchi, Solutions to shape and topology eigenvalue optimization problems using a homogenization method, *Int. J. Numer. Meth. Eng.* 35 (1992) 1487-1502.
- [15] Z.-D. Ma, N. Kikuchi, H.-C. Cheng, Topological design for vibrating structures, *Comput. Methods Appl. Mech. Eng.* 121 (1995) 259-280.
- [16] N. L. Pedersen, Maximization of eigenvalues using topology optimization, *Struct. Multidisc. Optim.* 20 (2000) 2-11.

- [17] O. Sigmund, J. S. Jensen, Systematic design of phononic band-gap materials and structures by topology optimization, *Philos. Trans. R. Soc. A-Math. Phys. Eng. Sci.* 361 (2003) 1001-1019.
- [18] Y. Li, X. Huang, F. Meng, S. Zhou, Topology optimization of 2D phononic band gap crystals based on BESO methods, in *Proc. 11th World Congr. Struct. Multidisciplinary Optim.*, Sydney, Australia 7-12 June 2015, pp. 157-161.
- [19] M. Ansari, A. Khajepour, E. Esmailzadeh, Application of level set method to optimal vibration control of plate structures, *J. Sound Vib.* 332 (2013) 687-700.
- [20] N. Olhoff, J. Du, Topological design for minimum dynamic compliance of structures under forced vibration, in G. Rozvany and T. Lewinski (Eds.), *Topology optimization in structural and continuum mechanics*, Springer, Wien, 2014, pp. 325-339.
- [21] M. Alvelid, Optimal position and shape of applied damping material, *J. Sound Vib.* 310 (2008) 947-965.
- [22] Z. Kang, X. Zhang, S. Jiang, G. Cheng, On topology optimization of damping layer in shell structures under harmonic excitations, *Struct. Multidisc. Optim.* 46 (2012) 51-67.
- [23] L. Shu, M. Y. Wang, Z. Fang, Z. Ma, P. Wei, Level set based structural topology optimization for minimizing frequency response, *J. Sound Vib.* 330 (2011) 5820-5834.
- [24] H. Zheng, C. Cai, G. Pau, G. Liu, Minimizing vibration response of cylindrical shells through layout optimization of passive constrained layer damping treatments, *J. Sound Vib.* 279 (2005) 739-756.
- [25] G. H. Yoon, J. S. Jensen, O. Sigmund, Topology optimization of acoustic-structure interaction problems using a mixed finite element formulation, *Int. J. Numer. Meth. Eng.* 70 (2007) 1049-1075.
- [26] J. Du, N. Olhoff, Minimization of sound radiation from vibrating bi-material structures using topology optimization, *Struct. Multidisc. Optim.* 33 (2007) 305-321.
- [27] X. Zhang, Z. Kang, Vibration suppression using integrated topology optimization of host structures and damping layers, *J. Vib. Control* 22 (2016) 60-76.
- [28] X. Zhang, Z. Kang, Topology optimization of damping layers for minimizing sound radiation of shell structures, *J. Sound Vib.* 332 (2013) 2500-2519.
- [29] S. Rothe, V. Ghaffari Mejlaj, S. C. Langer, T. Vietor, Optimal adaptation of acoustic black holes by evolutionary optimization algorithms, *Proc. Appl. Math. Mech* 16 (2016) 625-626.
- [30] O. Sigmund, A 99 line topology optimization code written in Matlab, *Struct. Multidisc. Optim.* 21 (2001) 120-127.
- [31] O. Sigmund, On the design of compliant mechanisms using topology optimization, *Mech. Struct. Mach.* 25 (1997) 493-524.
- [32] P. A. Feurtado, S. C. Conlon, Wavenumber transform analysis for acoustic black hole design, *J. Acoust. Soc. Am.* 140 (2016) 718-727.